

# Large Cyclic Poly(oxyethylene)s: Chain Folding in the Crystalline State Studied by Raman Spectroscopy, X-ray Scattering, and Differential Scanning Calorimetry

Jennifer Cooke,<sup>†</sup> Kyriakos Viras,<sup>‡</sup> Ga-Er Yu,<sup>§</sup> Tao Sun,<sup>§</sup> Takeshi Yonemitsu,<sup>§</sup> Anthony J. Ryan,<sup>||</sup> Colin Price,<sup>§</sup> and Colin Booth\*,<sup>§</sup>

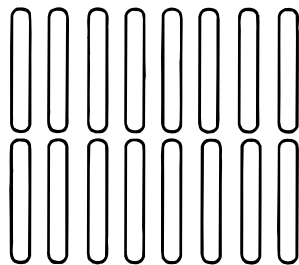
Manchester Materials Science Centre, UMIST, Grosvenor Street, Manchester M1 7HS, U.K., Physical Chemistry Laboratory, Department of Chemistry, National and Kapodistrian University of Athens, Panepistimiopolis, 157 71 Athens, Greece, Manchester Polymer Centre, Department of Chemistry, University of Manchester, Manchester M13 9PL, U.K., Department of Chemistry, University of Sheffield, Sheffield, S3 7HF, U.K., and CCLRC, Daresbury Laboratory, Warrington, WA4 4AD, U.K.

Received December 9, 1997; Revised Manuscript Received March 5, 1998

**ABSTRACT:** Crystalline cyclic poly(oxyethylene)s with number-average molar masses ( $M_n$ ) of 4000, 6000, and 10000 g mol<sup>-1</sup> were studied by wide-angle (WAXS) and small-angle (SAXS) X-ray scattering, high-frequency and low-frequency laser-Raman spectroscopy, and differential scanning calorimetry (DSC). The subcell of the crystalline cyclic polymers was the same as that of high-molar-mass poly(oxyethylene). Cyclic polymers of  $M_n = 4000$  or 6000 g mol<sup>-1</sup> crystallized in their twice-folded conformation under the conditions investigated, but the cyclic polymer of  $M_n = 10000$  g mol<sup>-1</sup> crystallized in a four-times-folded conformation when cooled from its melt and in a twice-folded conformation when crystallized slowly at high temperature. Comparison is made with the properties of corresponding linear poly(oxyethylene) dimethyl ethers.

## 1. Introduction

Comparative studies of the structures of crystalline linear and cyclic polymers are not common. Attention has been directed mainly toward uniform cyclic oligomers: for example studies of linear and cyclic alkanes by Wegner and co-workers,<sup>1–3</sup> of linear and cyclic oligourethanes by Höcker et al.,<sup>4</sup> and, related to the present study, of linear and cyclic oligo(oxyethylene)s (large crown ethers) by Yang et al.<sup>5,6</sup> Recently,<sup>7–9</sup> we have described investigations of the crystallinity of low-molar-mass cyclic poly(oxyethylene)s (number-average molar mass  $M_n = 1000–3000$  g mol<sup>-1</sup>), showing them to adopt the usual<sup>10</sup> crystal structure for poly(oxyethylene), i.e., alternate left and right-handed  $7/2$  helices packed into a structure with a monoclinic subcell. Of necessity, given the crystal structure, these small rings form lamellae in which parallel helix axes are twice folded, as shown schematically:

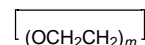


In work on uniform systems,<sup>6</sup> we have shown that this structure holds down to *cyclo*-E<sub>18</sub> ( $M = 792$  g mol<sup>-1</sup>). Here we describe the extension of our work to relatively

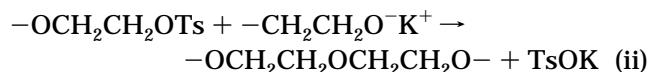
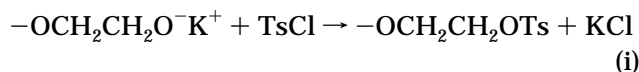
large cyclic poly(oxyethylene)s:  $M_n = 4000, 6000,$  and  $10000$  g mol<sup>-1</sup>.

Much is known about the crystallinity of low-molar-mass linear poly(oxyethylene)s, for example through early studies by X-ray scattering,<sup>11,12</sup> Raman spectroscopy,<sup>13,14</sup> and differential scanning calorimetry.<sup>15,16</sup> Poly(ethylene glycol)s [ $\alpha$ -hydro, $\omega$ -hydroxypoly(oxyethylene)s] with narrow molar mass distributions ( $M_w/M_n \leq 1.1$ ) and  $M_n \leq 20000$  g mol<sup>-1</sup> are available from a number of manufacturers. In the present work, these materials were used as precursors for preparation of cyclic poly(oxyethylene)s and poly(oxyethylene) dimethyl ethers.

We have recently described two methods of ring closure of poly(ethylene glycol)s, and cyclic polymers prepared by both routes were used in the present study. Reaction of poly(ethylene glycol) with tosyl chloride (*p*-toluenesulfonyl chloride, TsCl) at high dilution (ca.  $10^{-5}$  mol dm<sup>-3</sup> glycol) in the presence of solid KOH leads to closure by ether linkage:



The reactions involved are



This method was applied to the cyclization of PEG1000 by Vitali and Masci, with a reported yield of only 8%.<sup>17</sup> Under more favorable conditions, we have obtained a conversion of PEG1000 to cyclic poly(oxyethylene) of 80%<sup>8</sup> and have also prepared large uniform crown ethers in good yield by the same route.<sup>5,6</sup> The second method

<sup>†</sup> UMIST.

<sup>‡</sup> National and Kapodistrian University of Athens.

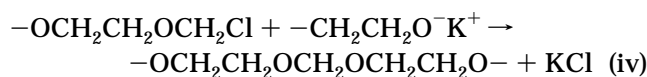
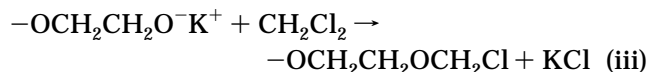
<sup>§</sup> University of Manchester.

<sup>||</sup> University of Sheffield and Daresbury Laboratory.

used in our laboratory<sup>18,19</sup> is the reaction of a poly(ethylene glycol) with dichloromethane (DCM) at high dilution in the presence of solid KOH, to attain ring closure via an acetal linkage:



In this case the reactions are



Conversions to cyclic polymer approaching 95% have been obtained.<sup>19</sup> The greater efficiency of this route reflects the extremely high reactivity of the chloroether formed in reaction iii, which ensures very rapid reaction in step iv even under the conditions of high dilution necessary to obtain efficient cyclization. In both procedures, at the dilutions used, a proportion of chain extension could not be avoided, but this polymer could be effectively eliminated by a simple fractional precipitation procedure.

Recently Ishizu and Akiyama have reported the cyclization of poly(ethylene glycol) by reaction of its sodium salt with 1,4-dibromobutane.<sup>20</sup> Remarkably they report cyclization with no chain extension even at relatively high concentrations of glycol ( $10^{-2}$ – $10^{-3}$  mol dm<sup>-3</sup>). We have repeated their procedure many times without success. Our method of proof of cyclization is unambiguous, being based on <sup>13</sup>C NMR spectroscopy and the absence of resonances characteristic of hydroxy end groups (see section 2.4 for details). We have consistently found almost complete recovery of precursor glycol. If there is no linking reaction, the absence of evidence of chain extension in the GPC curves of the products<sup>20</sup> is explained. Unfortunately Ishizu and Akiyama did not use a spectroscopic method to characterize their products.

The narrow molar mass distributions of the precursor polymers carry over to the cyclics, making them excellent materials for study of crystallinity. The methods used in the present work follow those used previously:<sup>7–9</sup> wide-angle X-ray scattering and high-frequency Raman spectroscopy to define crystal structure and packing, small-angle X-ray scattering and low-frequency Raman spectroscopy to define lamellar structure and chain conformation, and differential scanning calorimetry to monitor the extent of crystallinity and explore the thermodynamic properties of the lamellar crystals.

In what follows we use the notation LM, RE, and RA for, respectively, linear dimethyl ethers, cyclics with ether closure, and cyclics with acetal closure, and combine this with an indication of the number-average molar mass of the polymer. Thus samples 6000LM, 6000RA, and 6000RE derive from PEG6000 and are, respectively, its dimethyl ether, the cyclic polymer formed by acetal closure, and the cyclic polymer formed by ether closure. The three sets of samples are referred to as series LM, RA, and RE.

## 2. Experimental Section

**2.1. Cyclization.** Details of the methods used to cyclize the poly(ethylene glycol)s have been given recently.<sup>8,19</sup> It was

**Table 1. Cyclization of Poly(ethylene Glycol)**

precursor	conversion/%	
	acetal closure	ether closure
PEG4000	80	48
PEG6000	82	50
PEG10000	63	5

found that both methods gave acceptable conversion to cyclic polymer when using PEG4000 and PEG6000, but that the method of ether closure gave very poor results for PEG10000; see Table 1.

Here, as an example, we summarize the procedure for ether closure. Under dry nitrogen, a solution of PEG (5 g) and tosyl chloride (TsCl, 2–3 molar excess) in 100 cm<sup>3</sup> of a mixture of tetrahydrofuran and heptane (75/25 by volume) was added over 100 h to a dispersion of finely powdered KOH (85%, 5–7 g) in a second 100 cm<sup>3</sup> volume of the same mixed solvent held at 40 °C. After a further 24 h of stirring at 40 °C, the mixture was filtered and washed with water before the solvent was removed. A small portion of the product was analyzed by gel permeation chromatography (GPC: see section 2.3), and shown to be a mixture of the required cyclic polymer (50 mass %) plus chain-extended polymer impurity. This crude product was purified by fractional precipitation of the high-molar-mass chain-extended polymer from solution by adding a nonsolvent, taking care to achieve equilibrium in the separation stage. Details of the procedure, including examples of GPC curves obtained during purification, have been published previously.<sup>8,18,19</sup> With the high molar mass polymers, crystallization of the precipitate could complicate the fractionation process when using toluene (solvent) and heptane (nonsolvent). DCM plus heptane, which yielded a liquid precipitate, was preferred. The separation procedure was repeated until essentially all the high-molar-mass chain-extended polymer had been removed. The purified cyclic polymer, recovered from solution as a white crystalline product, was finally dried by heating under vacuum ( $10^{-4}$  mmHg, 60 °C, 24 h). Hydroxy end groups were undetectable by NMR spectroscopy (see section 2.3). Losses in the purification procedure resulted in recovery of some 50–70% of the cyclized polymer.

**2.2. Methylation.** The poly(ethylene glycol)s were methylated by reaction with iodomethane under alkaline conditions, as described previously.<sup>21,22</sup> For example, under dry nitrogen finely powdered KOH (85%, 2.3 g, 50-fold mole excess) in 20 cm<sup>3</sup> of chlorobenzene was stirred at room temperature, and iodomethane (0.35 g, 0.0025 mol) was added, followed by slow addition (25 min) of a solution of PEG6000 (5 g,  $8.3 \times 10^{-4}$  mol) in chlorobenzene (50 cm<sup>3</sup>), finally stirring for 8 h. After filtration, the solution was reduced to a small volume before taking it up in dichloromethane (100 cm<sup>3</sup>) and washing with distilled water ( $5 \times 30$  cm<sup>3</sup>) to obtain a negative test for iodide ion. After the organic phase was dried (MgSO<sub>4</sub>, 24 h), rotary evaporation followed by heating on a vacuum line ( $10^{-4}$  mmHg, 60 °C, 24 h) gave a white crystalline product. The GPC curve of the methylated product was essentially identical to that of the precursor. Conversion of hydroxy to methoxy end groups was in excess of 99%, as assessed by NMR spectroscopy (see section 2.3) and IR spectroscopy.<sup>21</sup>

**2.3. Gel Permeation Chromatography.** Several GPC systems were used during the course of the work. For example, a system with three PL-gel columns (two mixed B and one 500 Å, Polymer Laboratories) was used with *N,N*-dimethylacetamide eluent at 65 °C, while one with three  $\mu$ -Styragel columns (HR1, HR2, and HR3, Waters Associates) was used with THF eluent at 25 °C. In all cases the flow rate was 1 cm<sup>3</sup> min<sup>-1</sup>, detection was by differential refractometry, and volumes were referenced to internal standards. As expected,<sup>23</sup> the purified cyclic polymers eluted at higher volumes than their linear precursors; see Figure 1. Within experimental error the widths of the GPC curves were unchanged by cyclization and methylation: analysis gave values of  $M_w/M_n$  in the range  $1.07 \pm 0.03$  without correction for instrumental spreading; see Table 2.

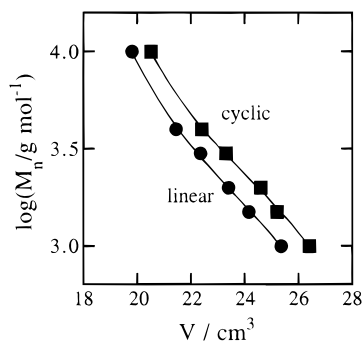


**Figure 1.** Logarithm of molar mass vs elution volume ( $V$ ) in GPC for cyclic and linear poly(oxyethylene)s. The GPC system had three  $\mu$ -Styragel columns (HR1 to HR3), and the eluent was THF.

**Table 2. Characterization of Cyclic and Linear Poly(oxyethylene)s by GPC**

sample	$M_w/M_n$	
	precursor	product
4000RA	1.05	1.06
6000RA	1.06	1.07
10000RA	1.10	1.10
4000RE	1.05	1.05
6000RE	1.06	1.09
4000LM	1.05	1.07
6000LM	1.06	1.06
10000LM	1.10	1.10

**2.4. NMR Spectroscopy.** NMR spectra were recorded by means of a Varian Unity 500 spectrometer operated at 125 MHz for  $^{13}\text{C}$  spectra, using solutions of ca. 5 wt % in  $\text{CDCl}_3$ . The number-average molar masses ( $M_n$ ) of the linear dimethyl ethers and the cyclic polymers with acetal closure were determined. The resonances of interest were as follows: (i) interior,  $-\text{OCH}_2\text{CH}_2\text{O}-$ ,  $\delta_{\text{C}} = 70.3$  ppm; (ii) ends  $-\text{OCH}_2\text{CH}_2\text{OH}$ ,  $\delta_{\text{C}} = 61.3$  ppm,  $-\text{OCH}_2\text{CH}_2\text{OH}$ ,  $\delta_{\text{C}} = 72.3$  ppm,  $-\text{OCH}_2\text{CH}_2\text{OCH}_3$ ,  $\delta_{\text{C}} = 71.7$  ppm, and  $-\text{OCH}_2\text{CH}_2\text{OCH}_3$ ,  $\delta_{\text{C}} = 70.1$  ppm; (iii) acetal,  $-\text{CH}_2\text{OCH}_2\text{OCH}_2-$ , 66.8 ppm. The intensities of the  $-\text{OCH}_3$  resonance at 58.8 ppm and the  $-\text{CH}_2\text{OCH}_2\text{OCH}_2-$  resonance at 95.5 ppm were less useful because of nuclear Overhauser enhancement (NOE) and relaxation effects. Depending on reaction conditions and chain length, the products of cyclization by acetal closure could contain multiple acetal links: e.g.,  $-\text{CH}_2\text{CH}_2\text{OCH}_2\text{OCH}_2\text{OCH}_2\text{CH}_2-$ . The characterization of these links will be described elsewhere.<sup>24</sup> The values of  $M_n$  obtained corresponded closely to those of their precursors (estimating the error to be  $\pm 4\%$ ), and to the manufacturer's specified values (i.e.  $M_n = 4000$ , 6000, and 10000  $\text{g mol}^{-1}$ ) which were accepted as appropriate. Because of their uniformity of composition, the molar masses of the cyclic polymers with ether closure could not be characterized in this way, apart from checking that their NMR spectra contained single peaks at 70.3 ppm. However, as described below, characterization of the cyclic polymers in the solid state by SAXS and low-frequency Raman spectroscopy yielded results which were entirely consistent (within experimental error) with these samples also having the same number-average chain lengths as their precursors.

**2.5. X-ray Scattering.** Measurements were made on beamline 8.2 of the SRS at the CCLRC, Daresbury Laboratory, Warrington, U.K. Details of the storage ring, radiation, camera geometry, and data collection electronics have been given elsewhere.<sup>25</sup> The camera was equipped with a multiwire quadrant detector (SAXS) located 3.5 m from the sample position and a curved knife-edge detector (WAXS) which covered  $70^\circ$  of the meridional arc at a radius of 0.3 m. A vacuum chamber placed between the sample and detectors reduced air scattering and absorption. The scattering pattern from an oriented specimen of wet collagen (rat-tail tendon) was used to calibrate the SAXS detector, and high-density poly-

ethylene, aluminum, and an NBS silicon standard were used to calibrate the WAXS detector.

Specimens were confined as thin films in a modified DSC pan<sup>26,27</sup> and could be melted and recrystallized while exposed to the X-ray beam. The temperature scale was calibrated by melting indium and lead and by the solid-state transition of anhydrous ammonium chloride and was checked against the melting temperatures of the polymers determined by conventional DSC (see section 2.6).

Results were obtained as intensity vs scattering angle  $2\theta$  (WAXS, normalized to  $\text{Cu K}\alpha$  radiation) or intensity vs scattering vector  $q = (4\pi/\lambda) \sin \theta$  (SAXS). Lamellar spacings ( $d$ ) were calculated from the position ( $q^*$ ) of the first-order peak in the SAXS plots of Lorentz-corrected intensity ( $Iq^2$ ) vs  $q$  (i.e.  $d = 2\pi/q^*$ ) and checked against the positions of higher-order maxima.

A measure of the total intensity of SAXS scattering was calculated as the area under the curve of Lorentz-corrected intensity vs  $q$  within the experimentally accessible range ( $q = 0.07$  to  $0.20$ ), i.e.

$$Q = \int_{0.07}^{0.20} I(q) q^2 dq \quad (1)$$

In the present experiments diffraction patterns from the long spacings were well sampled by the SAXS quadrant detector, although values of  $Q$  were found to vary between replicate experiments. This effect was caused by partial orientation of the sample. Orientation also meant that WAXS reflections could lie off meridian, making WAXS intensities obtained via the knife-edge detector very variable.

**2.6. Raman Spectroscopy.** Raman scattering at  $90^\circ$  to the incident beam was recorded for selected polymers by means of a Spex Ramalog spectrometer fitted with a 1403 double monochromator and with a third (1442U) monochromator operated in scanning mode. The light source was a Coherent Innova 90 argon-ion laser operated at 514.5 nm and 400 mW. Operating conditions for the low-frequency range were as follows: bandwidth  $\text{BW} = 1.0 \text{ cm}^{-1}$ , scanning increment  $\text{SI} = 0.05 \text{ cm}^{-1}$ , integration time  $\text{IT} = 4 \text{ s}$  for 4000RA and 6000RE;  $\text{BW} = 0.5 \text{ cm}^{-1}$ ,  $\text{SI} = 0.05 \text{ cm}^{-1}$ ,  $\text{IT} = 10 \text{ s}$  for 10000RA. The low-frequency scale was calibrated by reference to the 9.6 and  $14.9 \text{ cm}^{-1}$  bands in the low-frequency spectrum of L-cystine. Conditions for high-frequency spectra were as follows:  $\text{BW} = 3 \text{ cm}^{-1}$ ,  $\text{SI} = 1 \text{ cm}^{-1}$ ,  $\text{IT} = 2 \text{ s}$ . These spectra were taken before and after recording the low-frequency spectra, and served to confirm the stability of the samples under the conditions of the experiments, as well as giving structural information.

Routinely dried samples were held in the hollowed ends of stainless steel rods, in which they were melted and then cooled to room temperature to crystallize. Samples which underwent prolonged thermal treatment were confined in DSC pans and heated within the DSC instrument (see sections 2.7 and 3.3 for details) before mounting in rods for Raman spectroscopy.

Spectra were recorded with the samples at room temperature (ca.  $20^\circ \text{C}$ ). The exact temperature of the Raman experiment was unimportant for the present experiments, as the temperature derivative of frequency is known to be small for the LAM bands of poly(oxyethylene).<sup>14</sup>

**2.7. Differential Scanning Calorimetry.** A Perkin-Elmer DSC-4 was used. Known weights (ca. 5 mg) of dry samples were sealed into aluminum pans under nitrogen in a drybox. Thermal treatment (see section 2.7) was carried out in the instrument. Samples were usually heated at  $2^\circ \text{C min}^{-1}$ .

Values of the enthalpy of fusion ( $\Delta_{\text{fus}}H$ ) were obtained from peak areas, and apparent melting temperatures ( $T_{\text{m,app}}$ ) were obtained from positions of peak maxima. The power and temperature scales of the calorimeter were calibrated against the enthalpies of fusion and melting temperature of pure indium, and the temperature scale was checked against the melting points of organic standards covering the temperature range of interest. Correction for thermal lag was based on examination of certain standards at different heating rates and extrapolation to zero heating rate via plots of  $T_{\text{m,app}}$  against root heating rate. At the usual heating rate of  $2^\circ \text{C min}^{-1}$  the

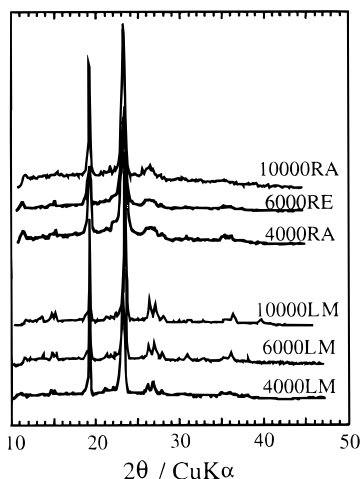


**Figure 2.** WAXS from (a) cyclic and (b) linear poly(oxyethylene)s crystallized and examined at 20 °C.

correction for poly(oxyethylene)s melting in the range 40–70 °C was  $-1$  °C.

**2.8. Crystallization of Samples.** Thermal treatment of the samples was as follows.

**(i) Stored.** Samples were taken from storage at  $-10$  °C and used without further treatment.

**(ii) Cooled (Room Temperature RT).** Samples were melted and then cooled slowly (ca.  $-5$  °C  $\text{min}^{-1}$ ) to room temperature (ca. 20 °C).

**(iii) Specified  $T_c$ .** Samples were melted, quenched at ca.  $-100$  °C  $\text{min}^{-1}$  to a specified crystallization temperature ( $T_c$ ), held at  $T_c$  for sufficient time to allow complete crystallization, and finally cooled to room temperature. If required, the rate of crystallization at high temperature was increased by inducing a high concentration of nuclei by self-seeding.<sup>15</sup>

**(iv) Annealed.** Quenched samples were heated to a temperature ( $T_a$ ) a few degrees below  $T_m$  and held at  $T_a$  for a specified time.

### 3. Results and Discussion

New results are described for five cyclic polymers (4000RA, 4000RE, 6000RA, 6000RE, and 10000RA) and three linear dimethyl ethers (4000LM, 6000LM, and 10000LM). Results published previously for shorter chains (1000–3000)<sup>7–9</sup> are used in discussion where appropriate.

**3.1. Crystal Structure.** The crystal structure was confirmed by WAXS and high-frequency Raman spectroscopy. The WAXS patterns (illustrated in Figure 2) and the Raman spectra (not shown) obtained for the crystalline cyclic polymers were essentially identical with those from their linear precursors. All WAXS patterns could be indexed to the accepted monoclinic subcell of crystalline high-molar-mass poly(oxyethylene),<sup>10</sup> indicating a crystal structure with alternating right and left-handed 7/2 helices. Similarly, the high-frequency Raman spectra were consistent with published spectra of crystalline poly(oxyethylene) and related oligomers,<sup>28–30</sup> particularly in the presence of spectral bands accepted as indicators of the helical conformation: e.g., at 291, 936, and 1231  $\text{cm}^{-1}$ .<sup>29,30</sup>

A consistent difference between the WAXS patterns from two types of polymer was the greater width of the reflections from crystals of the cyclic polymers. For the single reflections at 9.6 Å (the reflection at 11.6 Å is a composite), the difference in peak width at half-height was approximately a factor of 2. The same effect was seen in the poorer definition of the less intense reflections in the WAXS patterns from the crystalline cyclic

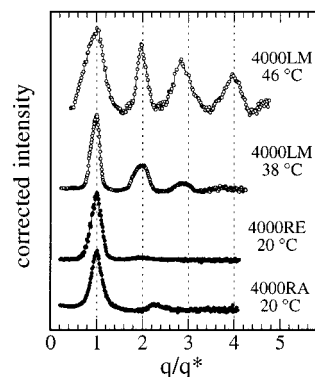


**Figure 3.** SAXS for cyclic and linear poly(oxyethylene)s:  $M_n = 4000$   $\text{g mol}^{-1}$ . Samples were cooled at  $50$  °C  $\text{min}^{-1}$  from the melt (70 °C) to the crystallization temperatures shown. Lorentz-corrected intensities are plotted against  $q/q^*$ , where  $q^*$  is the  $q$  value at the peak of the first-order reflection: i.e.,  $0.0238$  Å $^{-1}$  (4000LM, 46 °C),  $0.0465$  Å $^{-1}$  (4000LM, 38 °C),  $0.0484$  Å $^{-1}$  (4000RE, 20 °C), and  $0.0488$  Å $^{-1}$  (4000RA, 20 °C).

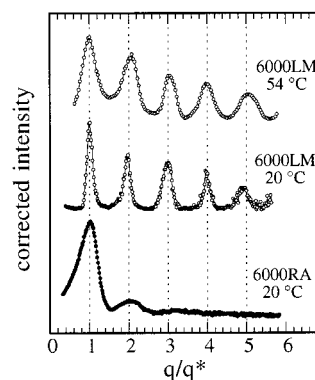


**Figure 4.** SAXS for cyclic and linear poly(oxyethylene)s:  $M_n = 6000$   $\text{g mol}^{-1}$ . Samples were cooled at  $50$  °C  $\text{min}^{-1}$  from the melt (70 °C) to the crystallization temperatures shown. Lorentz-corrected intensities are plotted against  $q/q^*$ , where  $q^*$  is the  $q$  value at the peak of the first-order reflection: i.e.,  $0.0138$  Å $^{-1}$  (6000LM, 54 °C),  $0.0321$  Å $^{-1}$  (6000LM, 20 °C), and  $0.0326$  Å $^{-1}$  (6000RA, 20 °C).

polymers (see Figure 2) and in the SAXS patterns (see next section). Presumably the effect is a result of the crystals formed from the cyclic polymers being consistently smaller in dimensions than those formed from the linear polymers.

**3.2. Small-Angle X-ray Scattering.** Examples of SAXS patterns obtained for crystalline samples of the cyclic and linear polymers are shown in Figure 3 ( $M_n = 4000$   $\text{g mol}^{-1}$ ), Figure 4 ( $M_n = 6000$   $\text{g mol}^{-1}$ ) and Figure 5 ( $M_n = 10000$   $\text{g mol}^{-1}$ ). Selected values of the lamellar spacing ( $d$ ) are listed in Table 3, where comparison is made with values of the contour length of the chain ( $l$ ) assumed to be in the usual helical conformation, i.e., calculated assuming an increment of 0.95 Å per chain atom (C or O, including end and linking groups).<sup>31</sup> Also included in Table 3 are the numbers of stems per molecule ( $s$ , a rounded value of  $(l/d) - 1$ , the assumption being that the helix axes are normal to the lamellar end planes, as is usual for poly(oxyethylene) lamellae<sup>11,12</sup>) and the corresponding values of the number of folds per molecule, i.e.,  $n = s$  for a cyclic molecule and  $n = s - 1$  for a linear molecule.

The SAXS patterns in Figures 3–5 are shown as Lorentz-corrected intensity vs  $q/q^*$ , where  $q^*$  is the  $q$  value at the peak of the first-order reflection. High order reflections ( $q/q^* > 4$  or 5) were not well resolved,

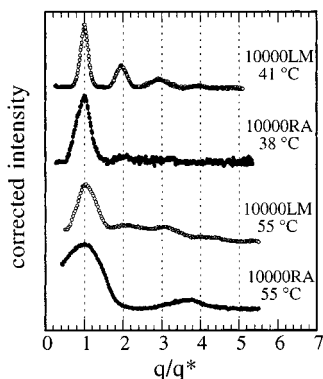


**Figure 5.** SAXS from cyclic and linear poly(oxyethylene)s:  $M_n = 10000 \text{ g mol}^{-1}$ . Samples were cooled at  $50 \text{ }^\circ\text{C min}^{-1}$  from the melt ( $70 \text{ }^\circ\text{C}$ ) to the crystallization temperatures shown. Lorentz-corrected intensities are plotted against  $q/q^*$ , where  $q^*$  is the  $q$  value at the peak of the first-order reflection: i.e.,  $0.0390 \text{ } \text{\AA}^{-1}$  (10000LM,  $41 \text{ }^\circ\text{C}$ ),  $0.0371 \text{ } \text{\AA}^{-1}$  (10000RA,  $38 \text{ }^\circ\text{C}$ ),  $0.0193 \text{ } \text{\AA}^{-1}$  (10000LM,  $55 \text{ }^\circ\text{C}$ ), and  $0.0189 \text{ } \text{\AA}^{-1}$  (10000RA,  $55 \text{ }^\circ\text{C}$ ).

**Table 3. Examples of Lamellar Spacings ( $d$ ), Molecular Lengths ( $l$ ), and Numbers of Folds ( $n$ ) Found for Cyclic and Linear Poly(oxyethylene)s<sup>a</sup>**

sample	$T_c/^\circ\text{C}$	$d/\text{\AA}$	$l/\text{\AA}$	$s$	$n$
4000LM	38	135	261	2	1
4000LM	46	263	261	1	0
4000RA	20	129	260	2	2
4000RE	20	130	259	2	2
6000LM	40	196	391	2	1
6000LM	54	398	391	1	0
6000RA	20	193	390	2	2
10000LM	41	161	650	4	3
10000LM	49	224	650	3	2
10000LM	55	326	650	2	1
10000RA	20	164	649	4	4
10000RA	38	169	649	4	4
10000RA	55	331	649	2	2

<sup>a</sup> Reproducibility of  $d$  (replicate crystallizations):  $\pm 3\%$ .

in particular for the cyclic polymers. It is assumed that the poor resolution is related to variation in lamellar thickness, with the consequent roughness approaching  $2\pi/q$  for the high orders. Generally, integer spaced reflections confirm a lamellar morphology. Given a reasonable estimate of error in locating maxima, e.g.,  $\pm 5\%$ , this is true of all the patterns except that for 10000RA crystallized at  $55 \text{ }^\circ\text{C}$  (see Figure 5). This discrepancy is allied to a very broad first-order peak, which is consistent with the sample containing mixed lamellae with chains in the twice-folded and four-times-folded conformations, the former being dominant.

As can be seen in Table 3, crystallization conditions were important in determining lamellar structure for all the linear polymers. This aspect was explored further, since results for poly(oxyethylene) dimethyl ethers of the particular chain lengths under investigation are less commonly found in the literature than those for their precursor glycols: e.g. results from Strasbourg<sup>11,12,15,16</sup> and from our own laboratory.<sup>32</sup> Comparable investigations have been reported by Cheng et al. for dimethyl ethers of 4250LM and 7100LM (present notation).<sup>33,34</sup> Studies of 3000LM by Cheng et al.<sup>35</sup> and Krimm et al.<sup>36</sup> and our own studies of 3000LE ( $E = \text{ethyl}$ )<sup>37</sup> lie somewhat outside the range of chain length of present interest. As shown in Figure 6, as the crystallization temperature was changed, transitions from one form to another were found, consistent with

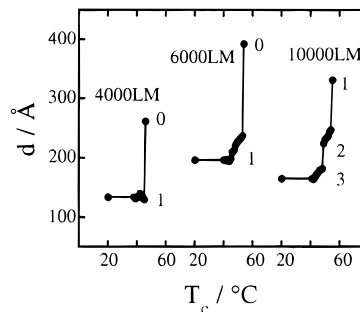


**Figure 6.** SAXS from linear poly(oxyethylene) dimethyl ethers: lamellar spacing ( $d$ ) vs crystallization temperature ( $T_c$ ). The extent of folding (number of folds,  $n$ ) is indicated.

changes in integral folding, either from one fold to unfolded (4000LM, 6000LM), or from three folds through two folds to one fold (10000LM). Crystals of 10000LM with unfolded chains were not formed under the conditions investigated.

The transition from folded to unfolded chains was rather sharp for the crystallization of 4000LM, occurring at  $T_c = 46 \text{ }^\circ\text{C}$ . For the longer chains, the transitions to the next lower integrally folded state (6000LM at  $T_c = 54 \text{ }^\circ\text{C}$ ; 10000LM at  $T_c = 49$  and  $54 \text{ }^\circ\text{C}$ ) were preceded by a temperature range in which the lamellae systematically thickened as  $T_c$  was increased. Similar effects have been described previously for OH-ended poly(oxyethylene), e.g., by Arlie et al.,<sup>11</sup> and for 7100LM by Cheng et al.<sup>34</sup> Overall, the results for our linear poly(oxyethylene) dimethyl ethers can be said to follow the general trends established in previous work,<sup>34</sup> and to differ little from the extensive work on hydroxy-ended analogues.

There are a number of possible explanations for the effect: crystal-stem tilting, nonintegral folding, and mixed integral folding within a lamella or lamella stack have all been identified. One mechanism is not exclusive of the others. The distribution of chain lengths in the samples is important in this respect, since chains may be incorporated into the same lamella in folded (longer chain) and unfolded (shorter chain) conformations, with very short chains being rejected entirely, as discussed and quantified previously.<sup>38</sup> To give an example, the width at half-height of the chain-length distribution of the present sample 10000LM,  $M_w/M_n \approx 1.07$ , is approximately 140 chain units, the number-average average chain length being only 227 chain units. The spread of chain lengths in relation to layer crystals has been illustrated elsewhere.<sup>39</sup> Assuming, for example, mixed integral folding, the fraction of chains in the various conformational states will vary with the rate of crystallization, which is controlled by the crystallization temperature. Selective chain unfolding or folding during isothermal crystallization will occur, and such mechanisms provide for formation of stable folded-chain crystals at higher temperatures than would be possible otherwise. Whatever the mechanism, the effect is unimportant in our experiments for the linear polymers with chain lengths below 136 oxyethylene units ( $M_n < 6000 \text{ g mol}^{-1}$ ) and, as described in the following paragraph, for all the cyclic polymers.

Lamellar spacings found for samples 4000RA and 4000RE were insensitive to crystallization conditions, as was expected since the twice-folded rings in these lamellae have stem lengths identical to those of PEG2000, which invariably crystallizes in an unfolded conformation.<sup>11,12</sup> Spacings found for 6000RA (6000RE

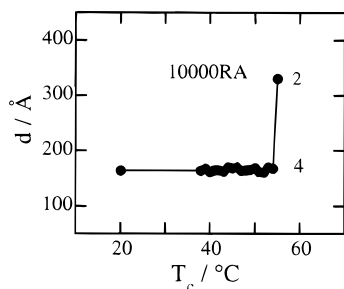


**Figure 7.** SAXS from cyclic poly(oxyethylene) 10000RA: lamellar spacing ( $d$ ) vs crystallization temperature ( $T_c$ ). The extent of folding (number of folds,  $n$ ) is indicated.

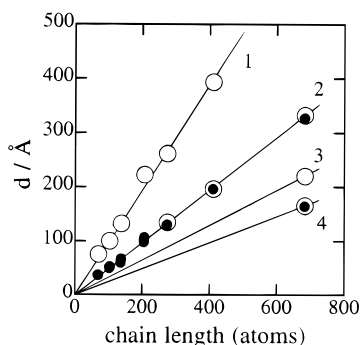


**Figure 8.** SAXS from cyclic and linear poly(oxyethylene)s: lamellar spacing ( $d$ ) vs chain length ( $z$ ) in chain atoms (C and O). The data points are for (O) linear polymers and (●) cyclic polymers. The numbers indicate the value of  $s$ , the number of crystal stems per molecule. The slopes of the lines drawn through the points are  $0.97/s \text{ \AA}$ .

was not investigated by SAXS) were also insensitive to the crystallization conditions investigated, e.g. cooling at  $50 \text{ }^\circ\text{C min}^{-1}$  to  $T_c = 20 \text{ }^\circ\text{C}$  resulted in crystals with spacings characteristic of twice-folded rings (see Figure 4). In contrast, the lamellar spacing obtained for sample 10000RA was changed by changing crystallization conditions. This is shown in Figure 7, where lamellar spacing is plotted against crystallization temperature. A sharp transition from crystals with rings in a four-times folded conformation to those with rings in the twice-folded conformation was found at  $T_c = 54 \text{ }^\circ\text{C}$ .

In Figure 8 SAXS results for the full series of cyclic poly(oxyethylene)s prepared and investigated in our laboratories ( $M_n$  from 1000 to 10000  $\text{g mol}^{-1}$ ) are brought together and compared with those obtained for their linear counterparts in a plot of lamellar spacing vs chain length in chain atoms. The present results are taken from Table 3, previous results from ref 9. The lines through the points have slopes in the range (0.96–0.97)/ $s \text{ \AA}$ , in fair agreement with the  $0.95/s \text{ \AA}$  found for uniform chains,<sup>31</sup> the slightly higher value for the polydisperse samples being consistent with slightly less dense lamellar surface layers.

Crystallization of a cyclic polymer in a four-times-folded conformation has not been reported previously. Possible conformations are discussed in section 4.

**3.3. Low-Frequency Raman Spectroscopy.** Only the cyclic polymers were investigated by Raman spectroscopy. Examples of spectra are shown in Figure 9. A broad band at  $80 \text{ cm}^{-1}$ , characteristic of crystalline poly(oxyethylene),<sup>14,40</sup> was present in each spectrum (not shown in Figure 9). The bands at very low frequencies ( $<10 \text{ cm}^{-1}$ ) were assigned to LAM-1. Initially all samples were crystallized by cooling rapidly to room temperature. LAM-1 frequencies ( $\nu_1$ ) found for these

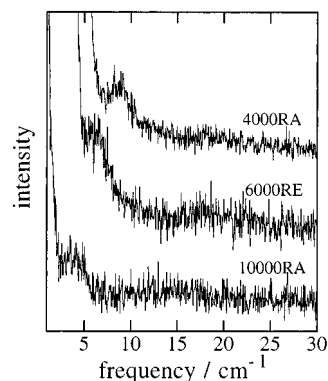


**Figure 9.** Low-frequency Raman spectra of cyclic poly(oxyethylene)s (as indicated) crystallized in the twice-folded conformation under the conditions shown in Table 4.

**Table 4. LAM-1 Frequencies ( $\nu_1$ ) of Cyclic Poly(oxyethylene)s**

sample	crystallization conditions	$\nu_1$ ( $\text{cm}^{-1}$ )	$n$
4000RA	annealed at $48 \text{ }^\circ\text{C}$	$8.3 \pm 0.5$	2
6000RE	annealed $51 \text{ }^\circ\text{C}$	$6.0 \pm 0.4$	2
10000RA	$T_c = 38 \text{ }^\circ\text{C}$	$7.4 \pm 0.4$	4
	self-seeded, $T_c = 56 \text{ }^\circ\text{C}$	$3.9 \pm 0.3$	2

rapidly cooled samples were some  $2\text{--}3 \text{ cm}^{-1}$  higher than expected in comparison with established results for linear poly(oxyethylene)s.<sup>14,41</sup> Satisfactory results were obtained either by annealing these samples at a high temperature or, alternatively, by initially crystallizing them at a high temperature; see Table 4 for details and LAM-1 frequencies. These results highlight the sensitivity of the LAM-1 frequency to perfection of lamellar structure, presumably through an increase in crystallinity (see section 3.4) and so of crystalline stem length. More subtle effects originating in interchain interaction have been identified.<sup>36,42</sup> In contrast, the spacing from SAXS was insensitive to the inner structure of the lamellae, being the sum of crystalline and noncrystalline layers of similar density.

It proved difficult to obtain a sample of wholly crystalline 10000RA in the twice-folded conformation. While it was relatively easy to obtain lamella spacings for this form in the real-time experiment (SAXS at Daresbury), where extents of crystallinity were low, this was not an option for Raman spectroscopy, where the sample had to be fully crystallized into the required form. Investigation by SAXS showed that annealing prior to melting did not result in unfolding. Instead the sample had to be heated to a temperature at which it started to melt, when self-seeded recrystallization in the less-folded state was possible. This is illustrated in Figure 10, which is a contour plot on a time- $q$  map of intensity as a crystalline sample of 10000RA was heated at  $10 \text{ }^\circ\text{C min}^{-1}$  from  $38$  to  $70 \text{ }^\circ\text{C}$ . For the Raman experiment, self-seeding by heating 10000RA to its melting point ( $58 \text{ }^\circ\text{C}$ ) followed by very slow crystallization at  $56 \text{ }^\circ\text{C}$  for 2 days, and then slow cooling ( $5 \text{ }^\circ\text{C h}^{-1}$ ) to room temperature gave the required result; see Figure 9 and Table 4.

In Figure 11 LAM frequencies from Table 4 are plotted against appropriate lamellar spacings from Table 3. Results from previous work for cyclic ( $M_n = 1500\text{--}3000 \text{ g mol}^{-1}$ ) and linear ( $M_n = 1000\text{--}3000 \text{ g mol}^{-1}$ ) poly(oxyethylene)s are included.<sup>9</sup> The excellent correlation of the parameters  $d$  and  $\nu_1$  across the wide range of samples, including 10000RA in its four-times-

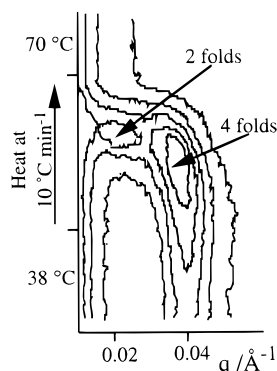


**Figure 10.** Contour plot on a time- $q$  map of intensity of X-ray scattering from a sample of 10000RA crystallized isothermally at 38 °C. The sequence along the ordinate is a period at 38 °C, then heating at 10 °C min<sup>-1</sup> to the melt at 70 °C, and finally a period at 70 °C. The scattering peaks corresponding to lamellae with the rings in the four-times-folded and twice-folded conformations are indicated.

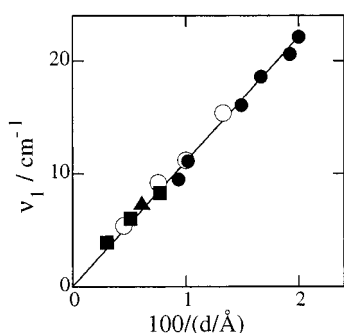


**Figure 11.** Low-frequency Raman spectroscopy of cyclic poly(oxyethylene)s. LAM-1 frequency ( $\nu_1$ ) vs reciprocal lamellar spacing ( $d$ , from SAXS): (●) low molar mass cyclics and (○) low molar mass linear dimethyl ethers from previous work;<sup>9</sup> (■) cyclics from this work.

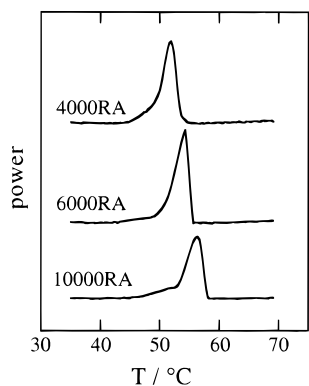


**Figure 12.** DSC curves for the RA series of cyclic poly(oxyethylene)s crystallized by quenching from the melt to 20 °C. The heating rate was 2 °C min<sup>-1</sup>. Baseline slopes have been adjusted. The power scales and zeros are arbitrary. Temperatures are corrected for thermal lag.

folded conformation, serves to confirm the interpretation of the SAXS results.

**3.4. Differential Scanning Calorimetry.** DSC curves (2 °C min<sup>-1</sup>) obtained for the RA series of cyclic polymers crystallized by quenching to 20 °C are shown in Figure 12. Tailing toward low temperatures is to be expected for samples with a distribution of chain lengths which have been rapidly crystallized. Heating at 2 °C min<sup>-1</sup> meant that samples annealed during the DSC experiment; hence, the peak relates to the most stable (least folded) crystals accessible. Samples crystallized

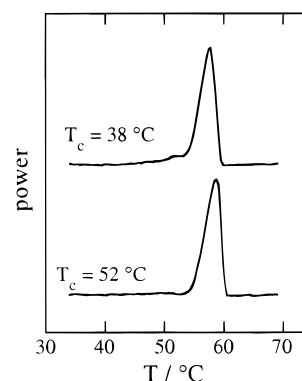


**Figure 13.** DSC curves for cyclic poly(oxyethylene) 10000RA crystallized by quenching from the melt to the temperatures indicated. The heating rate was 2 °C min<sup>-1</sup>. Baseline slopes have been adjusted. The power scales and zeros are arbitrary. Temperatures are corrected for thermal lag.

**Table 5. Melting Points ( $T_m$ ) and Enthalpies of Fusion ( $\Delta_{fus}H$ ) of Linear and Cyclic Poly(oxyethylene)s for a Heating Rate of 2 °C min<sup>-1</sup> <sup>a</sup>**

sample	crystallization conditions	$\Delta_{fus}H/J$ $g^{-1}$	$n$	$T_m/^\circ C$	$n$
4000LM	$T_c = 38^\circ C$ (2 h)	180	1	61	0
	$T_c = 55^\circ C$ (24 h)	174	0	62	0
6000LM	cooled (room temperature)	172	1	61	0
	$T_c = 55^\circ C$ (60 h)	178	0	63	0
10000LM	$T_c = 41^\circ C$ (1 h)	184	3	64	1
	$T_c = 49^\circ C$ (3 h)	186	2	64	1
	$T_c = 55^\circ C$ (24 h)	185	1	64	1
4000RE	all	134	2	53	2
6000RE	all	141	2	55	2
4000RA	all	131	2	52	2
6000RA	all	138	2	55	2
10000RA	$T_c = 38^\circ C$ (1 h)	140	4	58	2
10000RA	$T_c = 52^\circ C$ (overnight)	139	4	59	2
10000RA	$T_c = 56^\circ C$ (see section 3.3)	142	2	58	2

<sup>a</sup> Reproducibility:  $T_m, \pm 1^\circ C$ ;  $\Delta_{fus}H, \pm 5 J g^{-1}$ . Numbers of folds ( $n$ ) from SAXS and Raman spectroscopy, with allowance for annealing on slow heating (see text).

at higher temperatures gave DSC curves with single narrow peaks, see, for example, 10000RA,  $T_c = 52^\circ C$ , Figure 13. Corresponding DSC curves obtained for the linear dimethyl ethers (not illustrated) showed evidence of annealing, much as described by Buckley and Kovacs for the corresponding glycols.<sup>16</sup>

Values of  $\Delta_{fus}H$  and  $T_m$  are listed in Table 5. Conditions were chosen to match the SAXS experiments, although an inescapable difference was that the SAXS results were normally for low extents of crystallization, particularly when crystallizing at high temperatures, whereas the samples for DSC (as for Raman spectroscopy) were necessarily for samples crystallized to completion. In presenting the results (Table 5) it is assumed that  $\Delta_{fus}H$  relates (through Hess's law) to the state defined by SAXS (Table 3), whereas  $T_m$  relates to the annealed equilibrium (least folded) state for the cyclic polymers and the shorter linear polymers but, in conformity with the SAXS results, to the once-folded state for 10000LM, and the four-times-folded state for 10000RA (see Section 3.3).

On the basis of the simplest model of a lamellar crystal, the enthalpy of fusion should vary inversely with lamellar spacing according to

$$\Delta_{fus}H = \Delta_{fus}H^p - \frac{2\eta}{d} \quad (2)$$

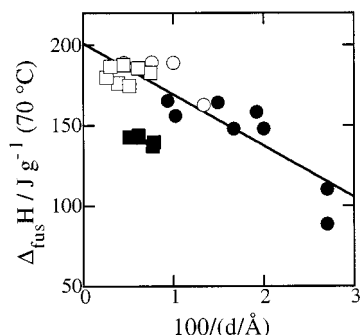


**Figure 14.** DSC of cyclic and linear poly(oxyethylene)s. Values of the enthalpy of fusion ( $\Delta_{\text{fus}}H$ ) corrected to  $70^\circ\text{C}$  vs reciprocal lamella spacing ( $d$ , from SAXS): (●) low-molar-mass cyclics and (○) low-molar-mass linear dimethyl ethers from previous work;<sup>9</sup> (■) cyclics and (□) linear dimethyl ethers from this work. The least-squares straight line excludes the data points for the high-molar-mass linear polymers.

where  $\eta$  is the excess surface enthalpy ( $\text{J m}^{-2}$ ). Because of the finite value of  $\Delta C_p$  for poly(oxyethylene), experimental values of  $\Delta_{\text{fus}}H$  should be corrected for the effect of melting range. The correction is<sup>43</sup>

$$\Delta_{\text{fus}}H(T_1) = \Delta_{\text{fus}}H(T_2) + 0.650(T_2 - T_1) - 0.00253(T_2^2 - T_1^2) \quad (3)$$

where temperatures are in  $^\circ\text{C}$ . Values of  $\Delta_{\text{fus}}H$  corrected to  $70^\circ\text{C}$  are plotted against  $1/d$  in Figure 14, the values of  $d$  corresponding to the numbers of folds listed adjacent to  $\Delta_{\text{fus}}H$  in Table 5. Results for low-molar-mass rings and chains ( $M_n = 1000\text{--}3000 \text{ g mol}^{-1}$ ) taken from ref 9 are included. As can be seen, the values of  $\Delta_{\text{fus}}H$  for the linear dimethyl ethers and the small cyclics fall approximately onto a straight line, and are clearly distinguished from the values found for the large cyclics in this work. A least-squares line through the data points for the linear and small cyclic polymers is shown in Figure 14. This extrapolates to a value for infinite lamellar thickness of  $\Delta_{\text{fus}}H^0 = 200 \text{ J g}^{-1}$ , which is within the range of values reported by other laboratories for poly(ethylene glycol)s,<sup>15,44</sup> i.e.,  $197\text{--}218 \text{ J g}^{-1}$ .

The low values found for all three of the present cyclics (compared with linear and small cyclic polymers at the same  $d$  spacing) has no obvious explanation in terms of chain conformation and lamellar morphology. It indicates a low degree of crystallinity within the lamellae. Whether this is a nonequilibrium effect related to the rate of crystallization or an equilibrium effect related to end melting<sup>45</sup> has yet to be determined. No doubt this result explains in some part the poorer resolution in WAXS and SAXS found for the cyclic polymers compared to the linear (see section 3.2).

For the simple model of a lamella, assuming no significant end-pairing effects<sup>45</sup> for the polydisperse chains, the melting point follows the equation

$$T_m = T_m^0 \left( 1 - \frac{2\gamma}{\Delta_{\text{fus}}H^0 d} \right) \quad (4)$$

where  $\gamma$  = excess surface Gibbs energy ( $\text{J m}^{-2}$ ),  $\Delta_{\text{fus}}H^0$  = thermodynamic enthalpy of fusion ( $\text{J m}^{-3}$ ), and  $d$  = lamellar thickness (m). In keeping with this model, a plot of melting point against reciprocal  $d$  spacing is shown in Figure 15. Results for the low-molar-mass cyclic and linear polymers are included. For this plot, values of  $d$  most appropriate for annealed samples are

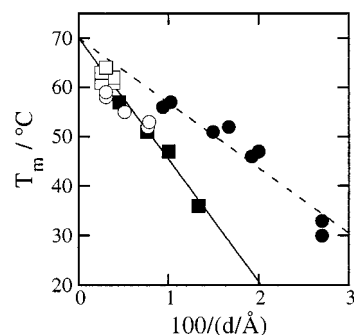


**Figure 15.** DSC of cyclic and linear poly(oxyethylene)s. Values of the melting point ( $T_m$ ) vs reciprocal lamella spacing ( $d$ , from SAXS): (●) low-molar-mass cyclics and (○) low-molar-mass linear dimethyl ethers from previous work;<sup>9</sup> (■) cyclics and (□) linear dimethyl ethers from this work. The least-squares straight lines pass through the data points for the low-molar-mass cyclics (dashed line) and the remaining data points (full line).

used (see the values of  $n$  listed in Table 5). The melting points for all the linear polymers fall approximately onto a straight line intercepting the ordinate at  $T_m^0 \approx 70^\circ\text{C}$ . Similarly, the melting points for the small rings can be extrapolated in an approximate way to the same intercept: see the dashed line in Figure 15. The value  $T_m^0 \approx 70^\circ\text{C}$  is much as expected: values in the range  $69\text{--}78^\circ\text{C}$  have been reported for poly(oxyethylene),<sup>15,44,46-48</sup> those at the bottom end of the range being obtained by extrapolation of results for linear poly(ethylene glycol)s.

As noted previously,<sup>9</sup> the melting points of the small cyclics are higher than those of linear polymers when compared at given  $d$  spacing. Given a similar relationship of  $\Delta_{\text{fus}}H$  to  $d$  spacing, the higher melting points found for the small cyclics can be attributed to lower entropies of fusion, through

$$T_m = \frac{\Delta_{\text{fus}}H}{\Delta_{\text{fus}}S} \quad (5)$$

This is as expected, since the linear and cyclic polymers are similarly conformationally restricted in the crystalline state, but the cyclic polymer is more conformationally restricted (compared with a linear polymer of the same length) in the melt state. The results for larger cyclic polymers add significantly to the picture. As can be seen in Figure 15, the melting points of the larger cyclic polymer coincide approximately with the straight line established for the linear polymers. The low enthalpies of fusion recorded for the large cyclics (see Figure 14) are consistent with disordered crystals, and hence a lowered entropy of fusion, and compensation of effects via eq 5.

#### 4. Chain Conformation in Crystalline 10000RA

As described above, cyclic poly(oxyethylene)s of molar mass  $1000 \leq M_n \leq 6000 \text{ g mol}^{-1}$  crystallize in the twice-folded conformation expected for a cyclic polymer in this range. In such crystals the folds will be predominantly to adjacent sites. However, cyclic polymer 10000RA crystallized at temperatures below  $55^\circ\text{C}$  enters the lamellae in a four-times-folded conformation.

Two possible conformations for 10000RA are shown in Figure 16. For simplicity, the conformations are represented with tight folds. However, it must be borne in mind that 10000RA is not uniform in chain length (see section 3.2 for discussion of this point) and that its

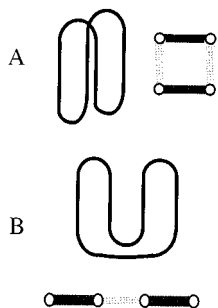


**Figure 16.** Schematic drawing to show possible conformations of cyclic polymer 10000RA in its four-times-folded conformation. Views perpendicular to and along the stems are shown. In the latter, the stems are indicated by circles, and the folds by dark shading (near surface) and light shading (far surface).

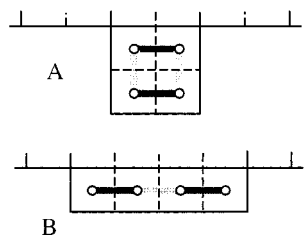


**Figure 17.** Schematic drawing to show possible secondary nuclei of cyclic polymer 10000RA in its four-times folded conformation: (A) as a bilayer and (B) as a monolayer. The view is along the stems, which are indicated by circles. The folds are indicated by dark shading (near surface) and light shading (far surface). Corresponding representations obtained by vertical inversion of the four-chain unit cell are not shown.

extent of crystallinity is not more than 70% (as judged by its enthalpy of fusion,  $140 \text{ J g}^{-1}$  compared with  $\Delta_{\text{fus}}^{\text{LP}} \approx 200 \text{ J g}^{-1}$ ). Consequently the folds are likely to be loose, and conformation B of Figure 16 cannot be dismissed out of hand.

In consideration of lamellar-crystal growth, models for secondary nucleation are shown in Figure 17: (A) as a bilayer; (B) as a monolayer. For these simple models, the Gibbs energies of secondary nucleus formation are

$$\Delta G_{\text{bilayer}} = 4bh\gamma_s + 8ab\gamma_e - 4abl\Delta g + 4f_1 \quad (6)$$

$$\Delta G_{\text{monolayer}} = 2bh\gamma_s + 8ab\gamma_e - 4abl\Delta g + 3f_1 + f_2 \quad (7)$$

where  $a$  and  $b$  are the dimensions of the chain in cross section, respectively parallel and normal to the growth face,  $l$  is the stem length,  $\gamma_s$  and  $\gamma_e$  are the lateral and fold surface Gibbs energies per unit area,  $\Delta g$  is the Gibbs energy of fusion (per unit volume),  $f_1$  is the Gibbs energy of forming an adjacent (short) fold, and  $f_2$  is the Gibbs energy of forming the nonadjacent (long) fold of the monolayer nucleus. In considering the path of lowest Gibbs energy of activation for nucleation, it can be seen that a bilayer is kinetically favored (i.e.  $\Delta G_{\text{bilayer}} < \Delta G_{\text{monolayer}}$ ) if

$$2bh\gamma_s < (f_2 - f_1) \quad (8)$$

while a monolayer is favored if the opposite is the case. Since terms involving  $\gamma_s$  are usually small, a bilayer is most likely. Similarly, lateral growth following first nucleation is faster for a bilayer nucleus, the consideration then being that  $f_1 < f_2$ .

## 5. Concluding Remarks

Over a series of papers,<sup>7-9</sup> we have studied the formation of lamellar crystals of low-molar-mass cyclic

poly(oxyethylene)s in which the rings had a twice-folded conformation. The present study has extended that work to larger ring sizes, in particular to a sample (10000RA) which crystallizes over a wide temperature range in a four-times-folded conformation. To the best of our knowledge, this is the first demonstration of such folding in a well-characterized synthetic cyclic polymer. Immediate interest lies in the nucleation processes in such a system, as touched upon in section 4. Spherulite growth rates will be determined and analyzed, and the results will be reported at a later date.

**Acknowledgment.** We thank Mr. P. Kobryn, Mr. K. Nixon, Mr. M. Hart, and Mr. B. U. Komanschek for help with the experimental work. The Engineering and Physical Research Council provided financial assistance and beamtime at the Daresbury Laboratory. Grants provided by the British Council (for K.V.) and ICI Paints Plc (for J.C.) enabled a detailed structural study of our materials.

## References and Notes

- Lee, K. S.; Wegner, G. *Makromol. Chem., Rapid Commun.* **1985**, *6*, 203.
- Lee, K. S.; Wegner, G.; Hsu, S. L. *Polymer* **1987**, *28*, 889.
- Leiser, G.; Lee, K. S.; Wegner, G. *Colloid Polym. Sci.* **1988**, *266*, 419.
- Heitz, W.; Höcker, H.; Kern, W.; Ullner, H. *Makromol. Chem.* **1971**, *150*, 73.
- Yang, Z.; Yu, G.-E.; Cooke, J.; Ali-Adib, Z.; Viras, K.; Matsuura, H.; Ryan, A. J.; Booth, C. *J. Chem. Soc., Faraday Trans.* **1996**, *92*, 3173.
- Yang, Z.; Cooke, J.; Viras, K.; Ryan, A. J.; Gorry, P. A.; Booth, C. *J. Chem. Soc., Faraday Trans.* **1997**, *93*, 4033.
- Viras, K.; Yan, Z.-G.; Price, C.; Booth, C.; Ryan, A. J. *Macromolecules* **1995**, *28*, 104.
- Sun, T.; Yu, G.-E.; Price, C.; Booth, C.; Cooke, J.; Ryan, A. J. *Polymer Commun.* **1995**, *36*, 3775.
- Yu, G.-E.; Sun, T.; Yan, Z.-G.; Price, C.; Booth, C.; Cooke, J.; Ryan, A. J.; Viras, K. *Polymer* **1997**, *38*, 35.
- Takahashi, Y.; Tadokoro, H. *Makromolecules* **1973**, *6*, 881.
- Arlie, J. P.; Spegt, P. A.; Skoulios, A. E. *Makromol. Chem.* **1966**, *99*, 160; **1967**, *104*, 212.
- Spegt, P. A. *Makromol. Chem.* **1970**, *140*, 167.
- Hartley, A. J.; Leung, Y.-K.; Booth, C.; Shepherd, I. W. *Polymer*, **1976**, *17*, 354.
- Viras, K.; Teo, H.-H.; Marshall, A.; Domszy, R. C.; King, T. A.; Booth, C. *J. Polym. Sci., Polym. Phys. Ed.* **1983**, *21*, 919.
- Viras, K.; King, T. A.; Booth, C. *J. Polym. Sci., Polym. Phys. Ed.* **1985**, *23*, 471.
- Buckley, C. P.; Kovacs, A. J. *Prog. Colloid Polym. Sci.* **1975**, *58*, 44.
- Buckley, C. P.; Kovacs, A. J. *Colloid Polym. Sci.* **1976**, *254*, 695.
- Vitali, C. A.; Masci, B. *Tetrahedron* **1989**, *45*, 2201.
- Yan, Z.-G.; Yang, Z.; Price, C.; Booth, C. *Makromol. Chem., Rapid Commun.* **1993**, *14*, 725.
- Yu, G.-E.; Sinnathamby, P.; Price, C.; Booth, C. *Chem. Commun.* **1996**, 31.
- Ishizu, K.; Akiyama, Y.; *Polym. Commun.* **1997**, *38*, 491.
- Cooper, D. R.; Booth, C. *Polymer* **1977**, *18*, 164.
- Cooper, D. R.; Leung, Y.-K.; Heatley, F.; Booth, C. *Polymer* **1978**, *19*, 309.
- Wright, P. V.; Beevers, M. S. In *Cyclic Polymers*; Semlyen, J. A., Ed; Elsevier: London, 1986; Chapter 3.
- Heatley, F.; Yu, G.-E.; Booth, C. To be published.
- Bras, W.; Derbyshire, G. E.; Ryan, A. J.; Mant, G. R.; Felton, A. Lewis, R. A.; Hall, C. J.; Greaves, G. N. *Nucl. Instrum. Methods Phys. Res. Sect. A*, **1993**, *326*, 587.
- Ryan, A. J. *J. Therm. Anal.* **1993**, *40*, 887.
- Bras, W.; Derbyshire, G. E.; Clarke, S.; Devine, A.; Komanschek, B. U.; Cooke, J.; Ryan, A. J. *J. Appl. Crystallogr.* **1995**, *28*, 26.
- Koenig, J. L.; Angood, A. C. *J. Polym. Sci., A-2* **1970**, *8*, 1787.
- Matsuura, H.; Fukuhara, K. *J. Phys. Chem.* **1987**, *91*, 6139.
- Matsuura, H. *Trends Phys. Chem.* **1991**, *1*, 89.
- Craven, J. R.; Zhang, H.; Booth, C. *J. Chem. Soc., Faraday Trans.* **1991**, *87*, 1183.

- (32) Beech, D. R.; Booth, C.; Dodgson, D. V.; Sharpe, R. R.; Waring, J. R. S. *Polymer* **1972**, *13*, 73.
- (33) Cheng, S. Z. D.; Chen, J.-H.; Heberer, D. P. *Polymer* **1992**, *33*, 1492.
- (34) Cheng, S. Z. D.; Wu, S. S.; Chen, J.-H.; Zhuo, Q.-H.; Quirk, R. P.; von Meerwall, E. D.; Hsiao, B. S.; Habenschuss, A.; Zschack, P. R. *Macromolecules* **1993**, *26*, 5105.
- (35) Cheng, S. Z. D.; Chen, J.-H.; Zhang, A.-Q.; Heberer, D. P. *J. Polym. Sci., Part B, Polym. Phys.* **1991**, *29*, 299. Cheng, S. Z. D.; Chen, J.-H. *J. Polym. Sci., Part B, Polym. Phys.* **1991**, *29*, 311.
- (36) Kim, I.; Krimm, S. *J. Polym. Sci., Part B, Polym. Phys.* **1997**, *35*, 1117; *Macromolecules* **1996**, *29*, 7168.
- (37) Fraser, M. J.; Marshall, A., Booth, C. *Polymer*, **1977**, *18*, 93. Fraser, M. J.; Cooper, D. R., Booth, C. *Polymer* **1977**, *18*, 852.
- (38) See, for example, Ashman, P. C.; Booth, C. *Polymer* **1975**, *16*, 892.
- (39) Marshall, A.; Domszy, R. C.; Teo, H.-H., Mobbs, R. H., Booth, C. *Eur. Polym. J.* **1981**, *17*, 885. Booth, C. In *Comprehensive Polymer Science, Vol. 1*; Booth, C.; Price, C., Eds.; Pergamon Press: Oxford, England, 1989; Vol. 1, Chapter 2, p 66.
- (40) Rabolt, J. F.; Johnson, K. W.; Zitter, R. N. *J. Chem. Phys.* **1974**, *61*, 504.
- (41) Campbell, C.; Viras, K.; Booth, C. *J. Polym. Sci., Polym. Phys. Ed.* **1991**, *29*, 1613.
- (42) Song, K.; Krimm, S. *J. Polym. Sci., Polym. Phys. Ed.* **1990**, *28*, 35.
- (43) Campbell, C.; Viras, K.; Richardson, M. J.; Masters, A. J.; Booth, C. *Makromol. Chem.* **1993**, *194*, 799.
- (44) Romankevich, O. V.; Frenkel, S. Ya. *Polym. Sci. U.S.S.R.* **1980**, *22*, 2647.
- (45) Flory, P. J.; Vrij, A. *J. Chem. Phys.* **1963**, *85*, 3548.
- (46) Beech, D. R. and Booth, C. *J. Polym. Sci., Part B* **1970**, *8*, 731.
- (47) Affifi-Effat, A. M. and Hay, J. N. *J. Chem. Soc., Faraday Trans. 2* **1972**, *68*, 656.
- (48) Rijke, A. M. and McCoy, S. *J. Polym. Sci., Part A-2* **1972**, *10*, 1845.

MA9717909